STEM CELLS TRANSLATIONAL MEDICINE℠

TISSUE ENGINEERING AND REGENERATIVE MEDICINE

Embryonic Stem Cell-Based Cardiopatches Improve Cardiac Function in Infarcted Rats

JEAN-PAUL VALLÉE,[a] MATHIEU HAUWEL,[b] MATTHIEU LEPETIT-COIFFÉ,[a] WANG BEI,[b] KARIN MONTET-ABOU,[a] PAOLO MEDA,[c] STEPHANY GARDIER,[a] PRISCA ZAMMARETTI,[b] THOMAS P. KRAEHENBUEHL,[b] FRANCOIS HERRMANN,[d] JEFFREY A. HUBBELL,[e] MARISA E. JACONI[b]

Key Words. Cardiac • Tissue regeneration • Stem cell transplantation • Embryonic stem cells

[a]Department of Radiology, Geneva University Hospitals and University of Geneva, Geneva, Switzerland; [b]Department of Pathology and Immunology and [c]Department of Cell Physiology and Metabolism, Faculty of Medicine, Geneva University, Geneva, Switzerland; [d]Department of Rehabilitation and Geriatrics, Geneva University Hospitals, Geneva, Switzerland; [e]Institute for Bioengineering, École Polytechnique Fédérale de Lausanne, Lausanne, Switzerland

Correspondence: Marisa E. Jaconi, Ph.D., Department of Pathology and Immunology, 1 rue Michel Servet, 1211 Geneva 14, Switzerland. Telephone: +41(0)22 37 95 257; Fax: +41(0)22 37 95 479; e-mail: marisa.jaconi@unige.ch

Received September 11, 2011; accepted January 23, 2012; first published online in SCTM *EXPRESS* March 7, 2012.

1066-5099/2012/$20.00/0

http://dx.doi.org/10.5966/sctm.2011-0028

ABSTRACT

Pluripotent stem cell-seeded cardiopatches hold promise for in situ regeneration of infarcted hearts. Here, we describe a novel cardiopatch based on bone morphogenetic protein 2-primed cardiac-committed mouse embryonic stem cells, embedded into biodegradable fibrin matrices and engrafted onto infarcted rat hearts. For in vivo tracking of the engrafted cardiac-committed cells, superparamagnetic iron oxide nanoparticles were magnetofected into the cells, thus enabling detection and functional evaluation by high-resolution magnetic resonance imaging. Six weeks after transplantation into infarcted rat hearts, both local ($p < .04$) and global ($p < .015$) heart function, as well as the left ventricular dilation ($p < .0011$), were significantly improved ($p < .001$) as compared with hearts receiving cardiopatches loaded with iron nanoparticles alone. Histological analysis revealed that the fibrin scaffolds had degraded over time and clusters of myocyte enhancer factor 2-positive cardiac-committed cells had colonized most of the infarcted myocardium, including the fibrotic area. De novo CD31-positive blood vessels were formed in the vicinity of the transplanted cardiopatch. Altogether, our data provide evidence that stem cell-based cardiopatches represent a promising therapeutic strategy to achieve efficient cell implantation and improved global and regional cardiac function after myocardial infarction. STEM CELLS TRANSLATIONAL MEDICINE *2012;1:248–260*

INTRODUCTION

Ischemic heart disease is a leading cause of morbidity and mortality in Western countries [1]. After myocardial infarction (MI), the ischemic area is typically replaced within a few weeks by a thin and stiff fibrotic scar layer, concomitantly to an enlargement of the left ventricular cavity and cardiac dysfunction. As the myocardium has limited intrinsic regeneration capacity after MI [2–3], stem cell transplantation represents a promising therapy to achieve functional improvement of cardiac function after myocardial infarction.

In preclinical studies centered on cell transplantation, infarct size, global and regional function, myocardial remodeling, and myocardial neoangiogenesis and perfusion have been improved in multiple species [4–5]. However, clinical trials have shown a potential but still uncertain benefit upon delivery of single-cell suspensions of mesenchymal or satellite stem cells [6–7]. Besides the importance of using securely committed cardiogenic cells, all preclinical and clinical studies emphasize the need to further improve the efficacy of cell transplantation and homing, in particular in a contracting myocardium, to achieve a successful clinical use of stem cell transplantation.

In particular, aside from the choice of the right cell source(s) for tissue regeneration, the optimal route for injection is still fiercely debated, including the need for additional growth factors that may favor or help tissue repair. Intravenous injection is relatively inefficient, as only a very small percentage of the transplanted cells are found in the infarct region. Intracoronary injection of stem cells may induce microvessel obstruction, restenosis, or acceleration of distal atherosclerosis. Intramyocardial injections, either transendocardial or transepicardial, have been associated with injuries, calcifications, local inflammation, and arrhythmia. To study the effect of cell therapy over a prolonged period, assessment of the amount of stem cells delivered to the infarct area is a requisite. Recently, stem cell labeling with iron oxide nanoparticles has been successfully imaged using magnetic resonance imaging (MRI) in the heart. This method was efficient to attest the correct delivery of stem cells after intramyocardial or intravenous injection, but, to our knowledge, it has not been used yet to assess the evolution of natural scaffolds patched on the myocardium [8–11].

Even if the list of candidate cells for cardiac regeneration has been growing over the past few

years, none of them appears as the obvious one [12–15]. This may be because several cell types are required to regenerate both muscular and vascular components of the heart wall [16–17]. Indeed, myocytes alone do not survive in a devascularized scar tissue [18], and a sole angiogenic treatment is often insufficient to yield stable functional improvements [16].

Embryonic stem cells (ESCs) have the attractive ability to differentiate into virtually any cell type of the body, to self-renew in vitro for an unlimited amount of time, and to be easily manipulated genetically [19]. Benefits of ESC therapy for the treatment of MI have been largely reported (reviewed in [14, 20]). However, the efficacy of cell engraftment is very low: $<$10% of the injected cells typically engraft, mainly because of cell death, and $<$2% appear to take on the in vivo fate of cardiac cells for tissue repair [21]. To achieve substantial cardiac regeneration, one has to provide a large number of cells in a supportive microenvironment to maximize cell retention, survival, differentiation into the appropriate cell type(s), and finally functional integration into the host tissue.

Recent attractive approaches now propose the generation of complex artificial cardiovascular tissue constructs in vitro with characteristics close to the endogenous heart tissue to be used as bioengineered cardiac grafts [22–27] (reviewed in [28]). Although such in vitro tissue engineering is a valuable method to decipher the mechanisms of cardiac histogenesis, its complexity may represent an obstacle to electrical coupling with the diseased tissue, and its cost tends to rule out large-scale clinical applications. Alternatively, one can rely on the natural ability of stem cells to self-organize and provide cardiac progenitors together with a supportive matrix to achieve in vitro [29–30] or in situ tissue engineering [31].

Several biomaterials are currently used for cardiac tissue engineering, such as fibrin, hyaluronic acid, collagen, or polyethylene glycol (PEG) [9, 32–36]. The ideal biomaterial should provide a scaffold to the degrading, infarcted extracellular matrix environment, biodegrade within a short period to release the incorporated cells, and let them colonize and remodel the tissue [37]. In our study, we used a fibrin matrix that is a natural polymer fully biocompatible and biodegradable [34, 38–39], and it is capable of supporting cell growth, migration, and differentiation. Its structure and degradation rate are easily adjustable, which makes fibrin hydrogel an ideal cell carrier for in situ tissue engineering. Here, we validated in rodents the efficacy of using 3D fibrin-based cardiac grafts as a treatment for myocardial infarction. We demonstrated that bone morphogenetic protein 2 (BMP2)-primed cardiac-committed ESCs seeded into these fibrin patches efficiently engraft and reduce remodeling and deterioration of cardiac functions following myocardial infarction.

Materials and Methods

ESC Culture and Cardiac Commitment

Mouse embryonic stem cells (mESCs) (CGR8 line, ECACC 95011018) and CGR8-GFP (a green fluorescent protein-transduced stable mESC line) were cultured as described elsewhere [40–41]. Briefly, cells were propagated in Glasgow modified essential medium (MEM) BHK-21 (Invitrogen, Carlsbad, CA, http://www.invitrogen.com), complemented with 1$\times$ MEM nonessential amino acids (Invitrogen), 1% (vol/vol) penicillin-streptomycin (Invitrogen), 2 mM sodium pyruvate (Invitrogen), 10% (vol/vol) fetal bovine serum (Invitrogen), 0.1 mM β-mercaptoethanol (Sigma-Aldrich, St. Louis, http://www.sigmaaldrich.com), and leukemia inhibitory factor (LIF) [41], in a humidified 5% CO_2 atmosphere at 37°C and maintained at $<$70% confluence to keep an undifferentiated phenotype. To induce cardiac differentiation, CGR8 cells were treated for 36 hours with 2.5 ng/ml BMP2 (R&D Systems, Minneapolis, http://www.rndsystems.com). Cardiac commitment was achieved by priming mESCs for 36 hours with 2.5 ng/ml BMP2 (gift from M. Puceat, INSERM, France) using the propagation medium as described above. Cells were then dissociated with trypsin and resuspended at 10^6 cells per 100 μl for the seeding into fibrin gels. The effect of BMP2 treatment on the expression of early cardiac markers was analyzed by quantitative polymerase chain reaction (Q-PCR) using primers described in [42].

Generation of ESC-Seeded Fibrin-Based Cardiopatches

Cells were first primed for 36 hours with 2.5 ng/ml BMP2 in the presence of LIF, as described [43]. Cells were then dissociated by trypsin treatment, and 3×10^5 BMP2-treated mESCs dissociated into single cells were seeded into 200-μl fibrin matrices. Non-cross-linked fibrin hydrogels were generated as previously described [44]. Briefly, hydrogels contained 5 mg/ml fibrinogen (Sigma-Aldrich, F4883), 20 units per ml thrombin (Sigma-Aldrich), 2.5 mM $CaCl_2$, and 1.5×10^6 cells per ml in TBS (containing per 1 l: 2.42 g Tris-base [20 mM], 8.75 g NaCl [150 mM], pH 7.4 with HCl) at pH 7.2. Polymerization was initiated by mixing 100 μl of fibrinogen/cells mix with 100 μl of thrombin/$CaCl_2$ mix in a 6 $\times$ 6 mm Lab-Tek chamber (Nalge Nunc International, Wohlen, Switzerland, http://www.nalgenunc.com).

Cell and Gel Loading with Superparamagnetic Iron Oxide

For magnetic resonance (MR) tracking of patches, labeling of single adherent mESCs was achieved with the MR contrast agent ferucarbotran (Resovist, Bayer AG, Leverkusen, Germany, http://www.bayerhealthcare.com) consisting of superparamagnetic iron oxide (SPIO) nanoparticles that were loaded into the cells by lipofection or magnetofection. Following the manufacturer's protocol to encapsulate materials by lipofection (transfection Kit-Effectene, Qiagen, Hilden, Germany, http://www1.qiagen.com), the cells were incubated for 24 or 48 hours with effectene and increasing concentrations of Resovist (2, 9, 14, and 28 mg/ml) and then washed with fresh culture medium. Conversely, for magnetofection, cells adherent on six-well-plate dishes were layered on top of six 200 mT permanent magnets, and wells were incubated for 30 minutes at 37°C with 14 μg of Resovist (42 μg of iron) in a total volume of 2 ml per well, a concentration that allowed the cells to optimally internalize the SPIO by pino-endocytosis. Free iron particles were washed out, and the medium was replenished.

To visualize cardiopatches by MRI in vivo, we first established the MRI requirements in vitro. We assessed that the basal value of T_2 for gels containing 300,000 mESCs without SPIO was 260 $\pm$ 90 ms. This T_2 decreased from 260 to 180 ms as SPIO load increased from 0.7 to 28 μg/ml (data not shown). A concentration of 7 μg/ml of SPIO in 2 ml of medium was thus chosen for mESC labeling to ensure a loss of T_2 of $\sim$30 ms. Because T_2 of the heart is $\sim$50 ms, these conditions were sufficient to obtain a good contrast in vivo between the cardiopatch and the left ventricular wall.

Evaluation of Iron Particle Loading

SPIO nanoparticle inclusion into the cells was assessed by Prussian blue staining and by electron microscopy. For electron microscopy analysis, 400,000 mESCs per well were seeded in a six-well plate. Three of six wells were incubated for 30 minutes with 7 μg/ml of Resovist in 2 ml of medium over a 200 mT permanent magnet. Cells were then washed, harvested, centrifuged (three wells per condition), and fixed in a pellet with 2.5% glutaraldehyde. Each cell sample was postfixed with 1% osmium tetroxide, dehydrated, and embedded in Epon resin. Ultrathin sections were then contrasted with 2% uranyl acetate and lead citrate according to Reynolds method [45]. Cells were then examined using a Philips CM10 transmission electron microscope (Philips, Eindhoven, The Netherlands, http://www.philips.com). Each of the two samples contained 1.1×10^6 cells.

Confocal Microscopy

CGR8-GFP [40] were embedded in a fibrin matrix as described above using 50:1 M ratio of fibrinogen/Alexa 647-conjugated fibrinogen (Molecular Probes, Eugene, OR, http://probes.invitrogen.com) and cultured in vitro for 1 week. Live confocal images of cell clusters were acquired at days 0, 2, 4, and 7.

Animal Preparation

Animal experimentation was performed in accordance with Swiss laws governing the care and use of animals for research. A total of 28 adult male Oncins France Strain A rats (Charles River Laboratories, Wilmington, MA, http://www.criver.com) weighing 250 $\pm$ 50 g were included in the study. Animals were anesthetized, intubated, and ventilated using a mixture of 2% isoflurane (Forene, Abbott, Abbott Park, IL, http://www.abbott.com) and 1 l/minute oxygen. Expiratory pressure, CO_2 level, and electrocardiogram (ECG) lead-I/V5 were continuously monitored. Myocardial infarction was induced as previously described [40]. After a left thoracotomy at the fifth intercostal space, the pericardium was incised and the heart was exposed to ligate the left anterior descending coronary artery by tying a piece of 6-0 silk suture around the vessel and the surrounding myocardium. Occlusion of the coronary artery was confirmed by the appearance of typical electrocardiogram changes (ST-segment elevation) as well as regional cyanosis and akinesia on the anterior ventricular area. A silk suture was also inserted around the coronary artery, but not tied, in control animals (sham operated). The cardiopatch was applied directly over the ischemic area and secured with fibrin glue (Baxter, Deerfield, IL, http://www.baxter.com). During the intervention all animals received an injection of xylocain as antiarrhythmic agent. The chest was closed and animals were allowed to recover in a heated cage. Postsurgical pain was controlled by infusing the wound with 1 ml of local anesthetic Carbostesin 0.5% (AstraZeneca, Zoug, Switzerland, http://www.astrazeneca.com) and giving subcutaneous injections of Temgesic (0.4 mg/kg) daily for 3 days. The mortality rate was $<$12%.

The rats were divided into the two major groups: a sham-operated group, also called normal (N), and a myocardial infarct (MI) group. Each of them were then subdivided into N + Cell-patch ($n = 4$) and MI + Cell-patch ($n = 5$) if fibrin patches contained cells loaded with SPIO nanoparticles, and into N + Iron-patch ($n = 5$) and MI + Iron-patch ($n = 5$) if fibrin patches contained only SPIO. Additional controls included nonengrafted animals (N, $n = 5$) and MI nonengrafted animals (MI, $n = 4$). At the end of the intervention all the animals received an injection of antiarrhythmia agent (xylocain) and carbostasin for local anesthesia on the chest scar.

During MRI, animals received the same 2% isoflurane and oxygen ventilated mixture. Vital parameters of the rat were monitored all along the MR procedure: temperature with an anal probe, respiration with a motion probe, and ECG with two electrodes positioned in the thoracic muscle (SA Instruments, Stony Brook, NY, http://www.i4sa.com). Fifty days after engraftment, rats were sacrificed by KCl intravenous injection via the femoral artery. Then the heart was surgically removed and fixed in formaldehyde solution before immunohistological process.

MRI

The rats were imaged using a 1.5 T Intera MR magnet (Philips) at days 2 (D2), 7 (D7), and 45 (D45) after surgical intervention. Animals were placed in prone position and head first. Their chest was placed over a 4.7-cm diameter surface coil (Philips). All the MR sequences were ECG triggered. The 2 hour per animal MR protocol consisted of 12 slices steady-state gradient echo (FFE) sequence (echo time [TE]/repetition time [TR]/flip angle [FA] = 7 ms/350 ms/50°, acquired pixel size = 0.2×0.3 mm^2, slice thickness = 2 mm, over 2 RR intervals [RR: time separating 2 consecutive R waves and corresponding to 1 cardiac cycle]) used for observation of iron oxide particles. A complementary-spatial modulation of magnetization (C-SPAMM) TAG preparation segmented cine FFE sequence (interTAG spacing = 1.25 mm, acquired pixel size = 0.6×1.8 mm^2, slice thickness = 3 mm, over 3 RR intervals) was also used for quantitative regional function study as previously described [46]. Ten short-axis slices were acquired to image the full heart. A seven-slice FFE cine sequence (acquired pixel size = 0.4×0.4 mm^2, slice thickness = 2 mm, over 2 RR intervals) was performed to evaluate the left ventricular ejection fraction (LV-EF), end-systolic volume (ESV), and end-diastolic volume (EDV) [47, 48]. A dose of 0.6 ml of gadolinium-diethylene-triaminepentaacetic acid (Gd-DTPA) contrast (Dotarem, Guerbet, Lanester, France, http://www.guerbet.com) per 400 g of rat body weight was injected intraperitoneally [46]. Ten minutes after the injection, an ECG-triggered multishot turbo field echo sequence was used for late enhancement imaging with the following parameters: TR/TE/inversion time = 7.6 ms/12 ms/300 ms inversion prepulse, turbo field echo factor = 6, FA = 45°, 416 $\times$ 512 matrix, 160-mm field of view, and 2 mm slice thickness over 3 RR intervals.

Evaluation of Cardiac Function, Left Ventricular Mass, and Patch Volume

For each of the seven slices of the cine FFE sequence, end-diastolic and end-systolic surfaces (cm^2) were manually contoured using the open-source software Osirix (http://www.osirix-viewer.com). End-diastolic volume (EDV, cm^3) and end-systolic volume (ESV, cm^3) of the left ventricle were determined as the sum of these surfaces and multiplied by the slice thickness parameter (0.2 cm). Left ventricular ejection fraction (LV-EF) was calculated as the ratio $EF = (EDV_{global} - ESV_{global})/EDV_{global}$. For left ventricular mass (LV mass) measurement, epicardial and endocardial borders of all slices were delineated. The mass was defined as the volume within the borders multiplied by a factor of 1.05, which represents an average myocardial specific density (g/ml) [48]. The patch volume was measured from manual drawing of the patch contours in the FFE T2* images using the region

of interest volume function of Osirix and a consensus between two observers. For the regional function study, each slice was divided into six sectors. Myocardial wall thickening was measured in each sector as the ratio of the thickness difference during systolic and diastolic cardiac phases by the end-diastolic thickness.

Circumferential Strains

C-SPAMM TAG images were analyzed using the ETC software [49] to determine in six sectors per slice the Lagrangian circumferential strain. The sectors were then classified in three groups (remote, infarct, and adjacent) based on the late imaging after gadolinium when there was, respectively, no enhancement, >50% enhancement, and <50% enhancement in the sector.

Histological and Immunohistological Analysis

The rats were sacrificed 50 days after engrafting the cardiopatch through intravenous injection of 2 ml of 3% potassium chloride, under general anesthesia using isoflurane. Hearts were excised, and the cardiac cavities were rinsed in phosphate-buffered saline (PBS) to remove blood and thrombi. The hearts were fixed with 10% formalin for 24 hours, embedded in paraffin, sectioned into 3 μm thickness slices, and stained with hematoxylin and eosin. Slices were then serially rehydrated in 100%, 95%, and 70% ethanol after deparaffinization with xylol. Endogenous peroxidase in samples was blocked with hydrogen peroxide, and antigens were retrieved on microwave for 15 minutes in 10 mM citrate buffer, pH = 6.0. Nonspecific binding was blocked with a 5% bovine serum albumin (BSA)/PBS solution for 15 minutes. Slices were stained at room temperature for 1 hour with rabbit anti-myocyte enhancer factor 2 antibodies (Santacruz SC-313, Santa Cruz Biotechnology Inc., Santa Cruz, CA, http://www.scbt.com) to identify cardiac cell nuclei, with goat anti-CD31 (PECAM-1, Santacruz SC-1506) to label vessel-like structures, or with antibodies specific for rMHC class II Ia antibodies to assess the infiltration of inflammatory cells like microglia/macrophages (OX6, 1:100, AbD Serotec, Raleigh, NC, http://www.abdserotec.com). Slices were then rinsed with PBS and incubated for 30 minutes at room temperature with an affinity-purified biotinylated secondary antibody (diluted 1:100 in 5% BSA/PBS), that is, anti-rabbit IgG and rat adsorbed anti-mouse IgG (Vector Laboratories, Burlingame, CA, http://www.vectorlabs.com). The slices were incubated for 30 minutes in avidin-biotin solution (Vectastin ABC Kit), and the reaction products were visualized with 3,3′-diaminobenzidine tetrahydrochloride dehydrate and H_2O_2 (Sigma-Aldrich). After washing with distilled water, counterstaining was performed with hematoxylin for 1 minute.

The tissues were observed and photographed with a Zeiss (Carl Zeiss, Feldbach, Switzerland, http://www.zeiss.com) Axioskop 2 Plus photomicroscope. Iron particles were visualized by Prussian blue (Sigma-Aldrich) staining by incubation into 5% potassium ferrocyanide (Sigma-Aldrich) and in 5% hydrochloric acid for 30 minutes, washed, counterstained with nuclear fast red, and examined under an inverted light microscope. Collagen fibers were stained by Landrum staining [50]. Iron particles were visualized by Prussian blue staining by incubation into 5% potassium ferrocyanide and in 5% hydrochloric acid for 30 minutes, washed, counterstained with nuclear fast red, and examined under a light microscope.

Statistical Analysis

The data are expressed as mean ± SD. Significant difference was determined by repeated-measurement ANOVA (Stata, StataCorp LP, College Station, TX, http://www.stata.com). The results were expressed as mean ± SD. The probability level of statistical significance was $p < .05$. To stratify animals into groups with comparable infarct severities, the treatment conditions and the sham operation for control rats were randomly assigned, and rats with infarcts smaller than 20% of the left ventricular wall were discarded ($n = 2$).

RESULTS

Generation and In Vitro Characterization of ESC-Seeded Cardiopatches

We first characterized the generation of fibrin-based cardiopatches in terms of pore size (see supplemental online Fig. 1a and 1b) for optimal, fast cell delivery in vivo. We analyzed fibrin degradation by BMP2-primed mESC seeded into 3D fibrin gels as single cells, small clusters, or embryoid bodies (EBs) (supplemental online Fig. 1c–1e). Partial fibrin degradation was observed around the proliferating GFP-expressing cell clusters already after 2 days of culture (supplemental online Fig. 1d, 1e), likely via the release of metalloproteinases. Indeed, we could detect by Zymogram analysis the expression of MMP-9 and MMP-2 for up to 7 days of gel culture (data not shown). We verified the BMP2-induced cardiac commitment by assessing the expression of cardiac genes such as MESP1, Nkx2.5, MEF2C, Tbx6, and GATA4 by Q-PCR. The expression of these markers was highly induced upon BMP2 treatment (supplemental online Fig. 2). When generating EBs, we observed a consistent increased and longer-lasting beating activity, scored over 2 weeks in culture (above 60% in BMP2-treated versus below 40% in control EBs, respectively).

To visualize the cardiopatches in vivo using MRI and then trace cells histologically post mortem, we first optimized cell loading with SPIO by comparing two loading methods: lipofection using a transfection agent and magnetofection using permanent magnets. Both methods were similar in terms of gross cell survival after SPIO uptake, intracellular fate, and content, as confirmed by trypan blue, Prussian blue staining (Fig. 1a, 1b), and electron microscopy (Fig. 1c–1e). SPIO appeared in the cytoplasm within endosomes, using both lipofection (Fig. 1c, 1d) and magnetofection (Fig. 1e). Some SPIOs were also visible at the surface and in the close periphery of the cells (data not shown). We did not observe alterations in cell proliferation and colony morphology of SPIO-loaded undifferentiated ESCs (Fig. 1a, 1b and supplemental online Fig. 3a, 3b), nor in the cardiac differentiation capacity within EBs (scored by the presence of contractile foci) at loading concentrations inferior to 10 μg/ml. We thus decided to use magnetofection for the rest of the experiments to achieve fast loading (1 hour instead of 1 day) and minimal SPIO dilution by cell proliferation before engraftment. Spots of iron staining remained still visible up to 1 week of differentiation within embryoid bodies (supplemental online Fig. 3c, 3d). To make sure that SPIO loading did not alter the function of mESC-derived cardiomyocytes in vitro, we recorded spontaneous $[Ca^{2+}]_i$ oscillations in isolated fluo-3 loaded cardiomyocytes and compared SPIO-loaded versus nonloaded cells (supplemental online Fig. 3e, 3f). No difference was found between control and SPIO-magnetofected mESC-derived EBs in terms of morphology

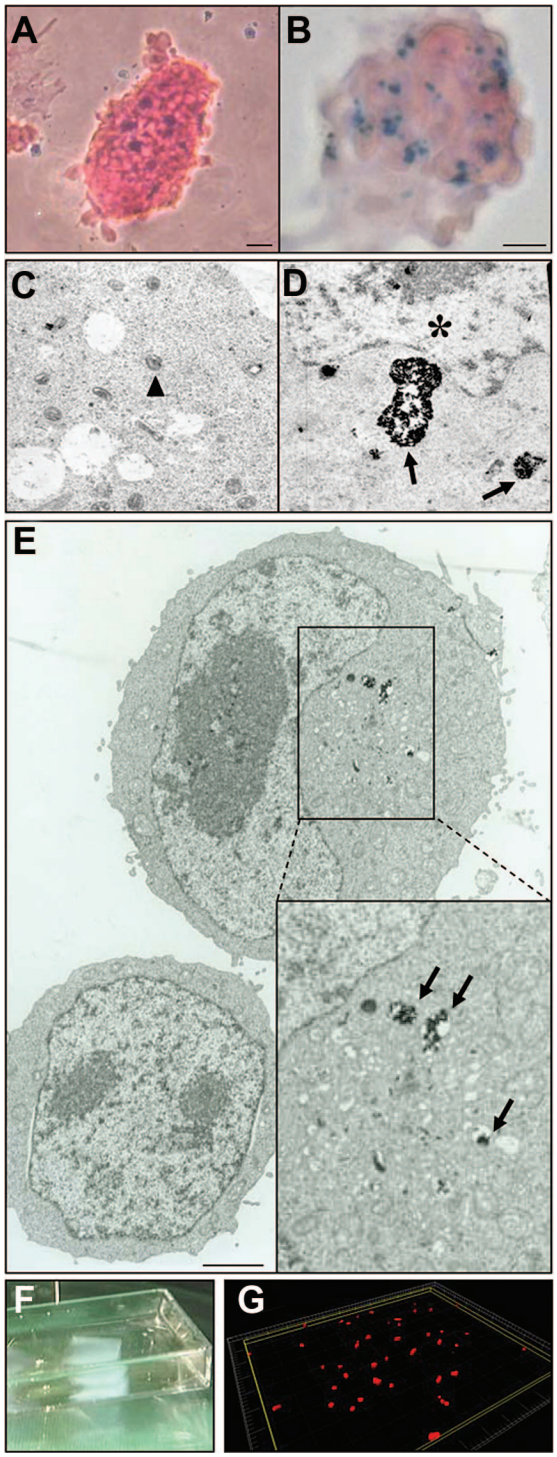

Figure 1. Evaluation of superparamagnetic iron oxide (SPIO) particle loading on mouse embryonic stem cells (mESCs). Magnetofected- or lipofected-ESC colonies (**[A]** and **[B]**, respectively) were stained with Prussian blue and contained similar amounts of SPIO. Electron microscopy pictures **(C, D)** confirmed the presence of iron particles within mESCs using both lipofection (**[C, D]**, 24 hours, 9 μg/ml) or magnetofection (**[E]**, 30 minutes, 7 μg/ml). Triangles, mitochondria; asterisk, nucleus; black arrows, iron-loaded endosomes. Scale bars = 1.2 μm **(E)** and 400 nm **(C, D). (F):** Image of a fibrin-based patch (5 × 5 × 1.5 mm), after polymerization of a 200 μl solution into a Lab-Tek multichamber and removal by lid lifting. **(G):** Example of cell distribution within a section of fibrin gel (300,000 cells per gel) upon 3D reconstruction of confocal images.

(supplemental online Fig. 3e, 3f, respectively), number of contractile areas scored within EBs (62 ± 10% versus 48 ± 20% of beating EBs, $\chi 2 = 1.32$, $p = .25$), or cardiomyocyte beating frequency (118 ± 18 versus 101 ± 28 beats per minute for control and labeled cells, respectively; $t = 1.73$, $p = .10$). Rhythmic $[Ca^{2+}]_i$ spikes in SPIO-labeled cardiomyocytes were also similar to those of control cells (supplemental online Fig. 3g).

Localization and Degradation of Cardiopatches Transplanted over Normal or Infarct Hearts

To assess the localization and degradation of the cardiopatches in vivo by MRI, either the gels were loaded with 7 μg/ml iron nanoparticles (termed "Iron-patch") or the iron nanoparticles were magnetofected into the BMP2-primed mESC prior to cell embedding into the fibrin gel (termed "Cell-patch"). In both cases, the cardiopatches were grafted onto normal (N, sham operated) or infarcted (MI) left ventricles, and MRI was performed over 45 days after animal surgery (Fig. 2A). At day 2, the patch volume was clearly visible in the epicardial region of the lateral wall, as assessed by the signal loss on the FFE T2* sequences (Fig. 2A). The patch volume was significantly larger on sham animals than animals with myocardial infarct ($p < .001$, Fig. 2B). In the four groups, the patch volume decreased between day 2 and day 7 ($p < .003$). At 45 days, the signal originated from the patch was barely detectable and not different between groups ($p > .29$).

The variability of the patch volumes measured by two independent observers was 57 ± 36% (mean ± SD) for the absolute volume. When considering only the volume reduction in percent from day 2 to day 7, the variability dropped to 27 ± 18%.

Cardiopatches Improved Local and Global Heart Function

To elucidate the effects of cardiopatches on normal and infarcted hearts, we performed high-resolution cine and tag MRI analysis of cardiac structure and function. At the difference of the FFE T2* sequences, no signal loss or artifacts were present in the patch region on both cine and tag images even 2 days after the engraftment. Cardiopatches loaded with either SPIO or cells did not induce modification of both the global or local cardiac function in the sham operated group ($p > .567$). On cine images, the myocardial wall thinning and the reduced wall thickening in the anterolateral wall of the mid and apical levels were well appreciated in the infarct groups (Fig. 3A, 3B). We assessed at 2, 7, and 45 days the evolution of the infarct size measured from the hyperintense signal on the delayed imaging after gadolinium injection (see supplemental online Fig. 4), as well as the left ventricular size (ESV and EDV) and global function (LV-EF) from the cine images. The infarct size was not different between MI, MI + Iron-patch, and MI + Cell-patch and did not change between 2 and 45 days, as reported in Table 1. In the infarct groups, the LV cavity increased over time, whereas the global function worsened by comparison to the sham animals ($p < .001$, see Table 1 and Fig. 3C). However, infarct rats treated with the Cell-patch (MI + Cell-patch) showed significantly attenuated left ventricular dilation at 45 days for both the ESV and EDV as compared with the Iron-patch group (MI + Iron-patch) (both $p < .001$). In addition, the LV-EF was improved in the MI + Cell-patch group by comparison to the MI + Iron-patch group at 45 days ($p = .015$).

The regional function was assessed from the circumferential strains derived from the tag images (see supplemental online Fig. 4B). A strong deformation of the tag grid was present during

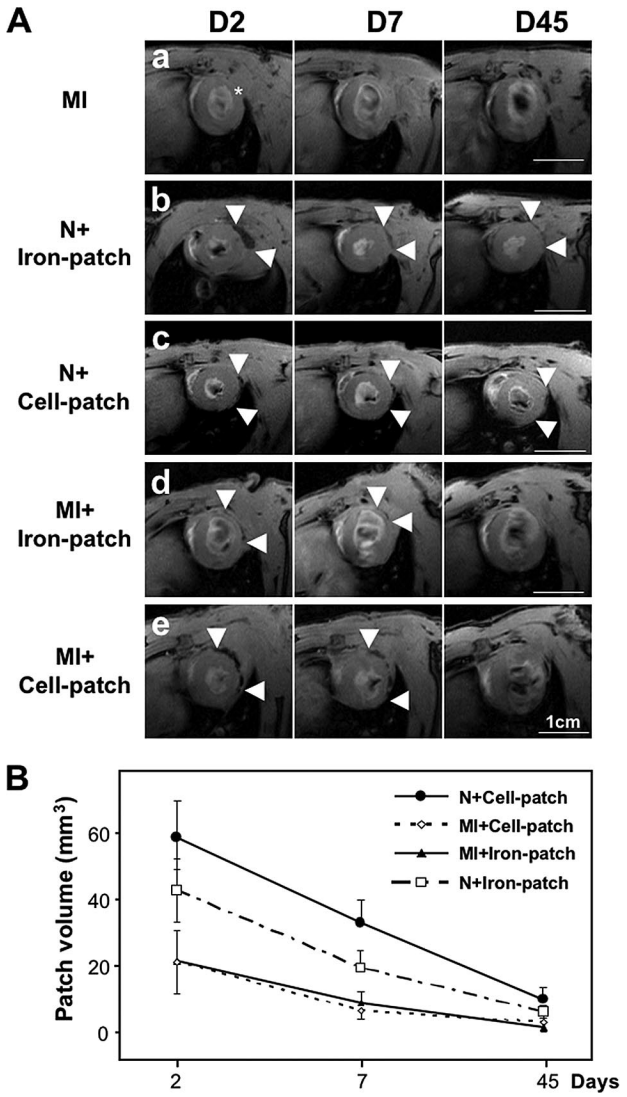

Figure 2. Analysis of the cardiopatch degradation after transplantation onto infarcted rat hearts using magnetic resonance imaging (MRI) at days 2, 7, and 45. **(A):** MRI over time of fibrin cardiopatches containing either superparamagnetic iron oxide (SPIO) nanoparticles alone or SPIO-loaded mouse ESCs, after grafting onto the left ventricles. Scale bars = 1 cm. * indicates center of the infarcted area; arrowheads show the limits of the patch extension. **(B):** Quantitative analysis of patch volumes shows a decrease over time for the different patch conditions. Abbreviations: D, day; MI, myocardial infarction; N, normal.

systole in remote areas, whereas there was no tag displacement in the infarct regions. As reported in Table 2, an ANOVA with repeated measures adjusted for the effects of the treatment, the time, the slice level, the sector classification, and their interactions demonstrated a global effect of the sectors classification ($p < .001$), attesting to the efficacy of the infarct induction but no effect of the day or slice level. It also demonstrated a global effect of the treatment ($p < .001$). No strain difference was found between the MI + Iron-patch and the MI groups. Therefore, the MI + Iron-patch and MI groups were pooled together and compared with the MI + Cell-patch group to investigate the effect of cell treatment on myocardial infarction. As indicated in Table 2B, the circumferential strain was significantly increased in the endocardium ($p < .008$) and in the midwall ($p < .026$) for the MI + Cell-patch, by comparison to the pooled MI group. Such a benefit was also present, but less pronounced, for the epicardium strain of the MI + Cell-patch ($p < .072$). There was also no interaction between the different effects (treatment, time, slice, and sector type). Interestingly, the Cell-patch-dependent improvement of global and regional cardiac parameters was observed already at day 2 and in all myocardial sectors, whether infarcted, adjacent, or remote.

Cardiopatch-Delivered Cardiac-Committed Cells Colonize the Infarcted Myocardium

To better understand the functional improvement as assessed by MRI, we histologically analyzed the rat hearts at 45 days to evaluate cell engraftment, localization, and fate (Fig. 4), as well potential stem cell-dependent neovascularization (Fig. 5). Lendrum staining enabled appreciation of the structure of the preserved force-generating cardiomyocytes and of the collagen content deposited in the infarcted area (Fig. 4C). We detected a dramatic left ventricular wall thinning associated with an extended, transmural fibrous scar, typical for a permanent coronary occlusion on infarcted hearts. Myocardium hypertrophy appeared to be more prominent in nontreated, sham-operated animals as compared with animals that received an Iron-patch or a Cell-patch. A thin fibrous layer of connective tissue was observed around the hearts resulting from pericardium healing, but no fibrin gel was visible 45 days after grafting. At higher magnification, Lendrum staining showed a massive muscular fiber loss, replaced by collagen fibrils both in treated and nontreated animals (Fig. 4C, 4D).

Clusters of MEF2-positive cells with colocalized Prussian blue staining were found in the fibrotic area in treated animals, whereas few or no MEF2-, Prussian blue-positive cells could be detected in nontreated animals (Fig. 4C versus 4D). We observed that mESCs did not penetrate the tissue in noninfarcted hearts but remained in the outer connective tissue where they differentiated into MEF2-positive cells (Fig. 4B).

Cardiopatch-Induced Neovascularization

A high density of CD31-positive cells and small vessels was consistently observed both in cardiopatch-treated normal or infarcted myocardium (N + Cell-patch and MI + Cell-patch, Fig. 5A, 5B), as opposed to Iron-patch-treated hearts (Fig. 5C). Capillary density within the myocardial tissue was not changed in sham-operated animals treated with Iron-patch (data not shown), where neoangiogenesis occurred exclusively in the surrounding connective tissue (Fig. 5A). Prussian blue pearls did not associate with blood vessels in either sham or infarcted animals.

Discussion

Our goal was to stimulate in situ the regeneration and repair of infarcted hearts by using fibrin-based cardiopatches embedded with cardiac-committed mESCs. The present work indicates the safety and efficacy of grafting fibrin-based cardiopatches over normal or infarcted rat left ventricles, in comparison with grafting of patches exclusively loaded with SPIO nanoparticles. Using high-resolution MRI, we demonstrated that cell patches led to an improvement of both local and global heart function over a 6-week period, a result consistent with a significantly attenuated left ventricular dilation, in comparison to control infarcted hearts, whether receiving SPIO-loaded patches or not.

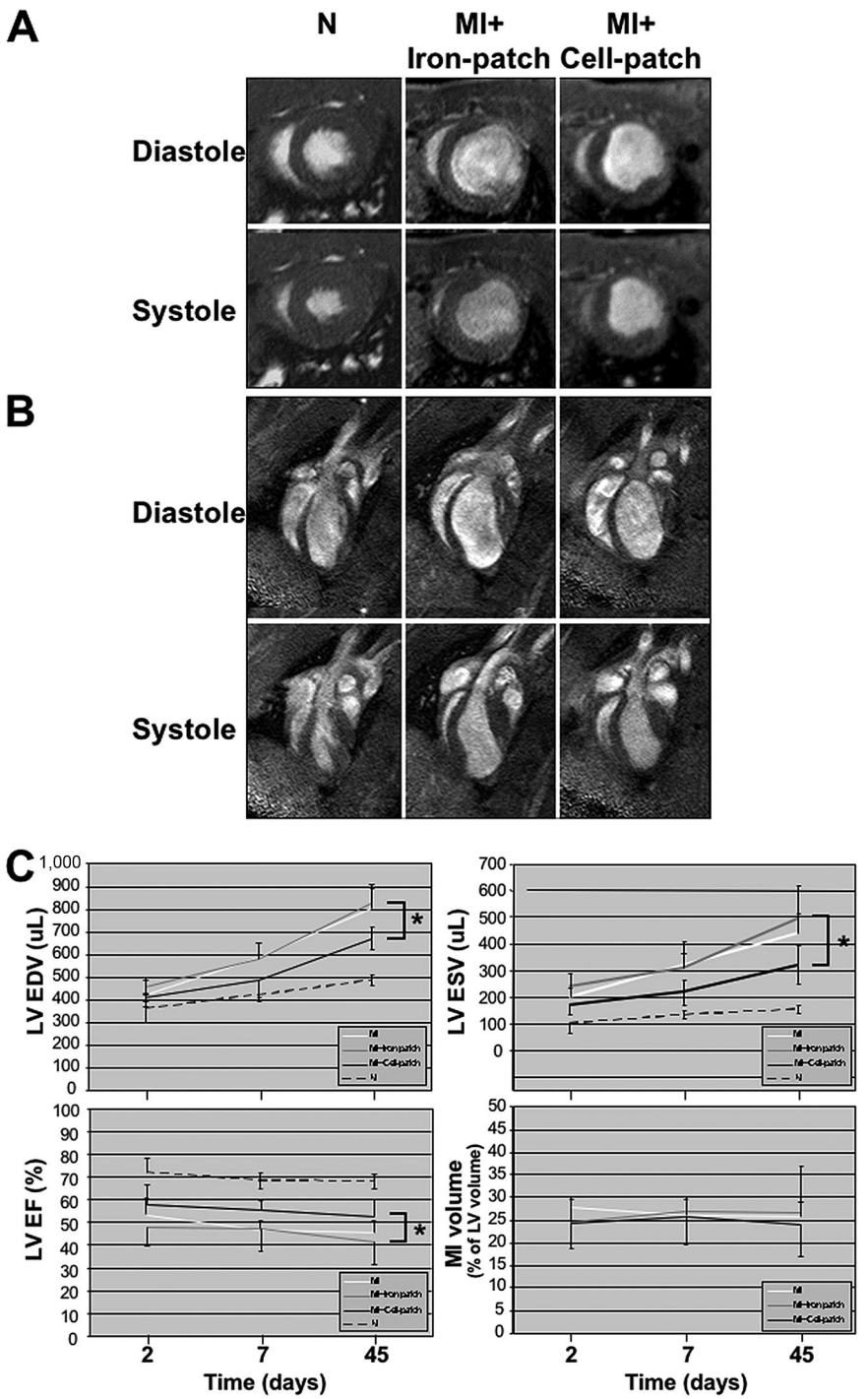

Figure 3. Magnetic resonance imaging analysis of cardiac parameters upon transplantation of cardiopatches loaded with either superparamagnetic iron oxide nanoparticles (Iron-patch) or bone morphogenetic protein 2-primed mouse embryonic stem cells with incorporated iron nanoparticles (Cell-patch). **(A, B):** Representative images of short-axis **(A)** and four-chamber views **(B)** in diastole and systole. Scale bars = 1 cm. **(C):** Rats treated with Cell-patch showed attenuated left ventricular dilation at 45 days as compared with the Iron-patch, as well as significantly improved end-diastolic and end-systolic volumes. No significant difference in infarct size was detected between the between the Iron-patch and the Cell-patch between 2 and 45 days. ∗ denotes $p < .05$. Abbreviations: EDV, end-diastolic volume; EF, ejection fraction; ESV, end-systolic volume; LV, left ventricle; MI, myocardial infarction.

One particularity of our study relies on the use of MRI as a technique considered more accurate and reproducible than echocardiography to measure cardiac function and volume. Some previous studies have already demonstrated the potential of MRI for cardiac function assessment in preclinical studies [8–11, 51, 52]. Recently, one group demonstrated the therapeutic effect of nude biodegradable poly(glycerol sebacate) scaffolds on myocardial infarct in rats but also the detrimental effect of other types of scaffolds [53]. In our study, we were able to show the absence of detrimental effects of our 3D fibrin matrix on heart contraction

Table 1. Evolution of cardiac parameters assessed by MRI over the three follow-up time points

	Days					
	2		7		45	
N ($n = 5$)						
LV-EF (%)	68.2 ± 2.2		68.1 ± 1.9		65.5 ± 1.8	
ESV (μl)	140.7 ± 22.9		151.4 ± 7.7		201.3 ± 8.6	*/**
EDV (μl)	440.4 ± 50.3		475.5 ± 26.8		585.6 ± 36.7	*/**
LV mass (mg)	468.4 ± 42.5		513.1 ± 43.4	*	668.7 ± 19.7	*/**
N + Iron-patch ($n = 5$)						
LV-EF (%)	71.8 ± 6.3		68.3 ± 3.5		68.1 ± 3.1	
ESV (μl)	103.2 ± 37.4		132.9 ± 14.8		154.8 ± 15.6	*
EDV (μl)	359.6 ± 62.9		422.2 ± 28.7		486.0 ± 24.6	*/**
LV mass (mg)	455.7 ± 92.9		472.0 ± 79.6		600.4 ± 60.0	*/**
N + Cell-patch ($n = 4$)						
LV-EF (%)	71.5 ± 7.4		66.6 ± 5.7	*	70.2 ± 5.2	
ESV (μl)	116.1 ± 54.7		155.4 ± 50.4	*	160.8 ± 40.5	*
EDV (μl)	392.6 ± 114.0		462.1 ± 95.1	*	540.2 ± 100.0	*
LV mass (mg)	497.7 ± 66.6		541.3 ± 74.7		581.1 ± 106.1	
MI ($n = 4$)						
Infarct size (%)	27.6 ± 2.1		26.2 ± 3.4		25.6 ± 3.4	
LV-EF (%)	53.5 ± 7.0	◊	46.6 ± 4.5	◊	45.5 ± 5.4	*/◊
ESV (μl)	197.5 ± 35.9	◊	319.3 ± 44.4	*/◊	438.7 ± 76.6	*/**/◊
EDV (μl)	426.2 ± 59.8		586.1 ± 64.3	*/◊	802.6 ± 86.4	*/**/◊
LV mass (mg)	441.3 ± 31.7		492.3 ± 16.1		663.6 ± 119.6	*
MI + Iron-patch ($n = 5$)						
Infarct size (%)	24.4 ± 5.6		26.9 ± 3.3		26.4 ± 10.5	
LV-EF (%)	48.1 ± 8.3	◊	47.1 ± 10.0	◊	41.6 ± 10.3	*/◊
ESV (μl)	238.5 ± 51.5	◊	311.0 ± 96.0	◊	491.6 ± 126.1	*/**/◊
EDV (μl)	457.0 ± 43.9		577.5 ± 69.0	*/◊	824.8 ± 86.1	*/**/◊
LV mass (mg)	483.4 ± 70.8		472.7 ± 7.9		628.8 ± 87.8	*/**
MI + Cell-patch ($n = 5$)						
Infarct size (%)	24.3 ± 5.8		25.8 ± 6.2		23.8 ± 7.1	
LV-EF (%)	58.1 ± 8.6	◊	55.2 ± 4.4	◊	52.4 ± 8.0	◊
ESV (μl)	172.6 ± 38.6		219.1 ± 47.9	*/◊	319.7 ± 71.1	*/**/◊/††
EDV (μl)	412.3 ± 18.5		486.2 ± 77.0		668.6 ± 49.0	*/**/◊/†/††
LV mass (mg)	468.9 ± 71.3		513.1 ± 63.9		668.7 ± 77.4	*/**

Significant differences as a function of time and groups are indicated as follows: *, $p < .05$ versus 2 days; **, $p < .05$ versus 7 days; ◊, $p < .05$ versus all normal groups; †, $p < .05$ versus MI; ††, $p < .05$ versus MI + Iron-patch.
Abbreviations: EDV, end diastolic volume (μl); ESV, end-systolic volume (μl); LV mass, left ventricular mass (μl); LV-EF, left ventricular-ejection fraction (%); MI, myocardial infarction; MRI, magnetic resonance imaging; N, normal.

using both cine and tag MRI. In addition, we checked early in the time course of the model, that is, right after the induction of the infarct, that all the groups had a similar size of myocardial infarct. This ensures that all the groups are well balanced without differences in the generated infarct size, related to variability of the level of coronary occlusion. Such verification is usually not performed in most of the published studies. Only recently, a few publications have reported the measurement of infarct area by MRI right after the infarct induction using delayed gadolinium enhancement [8, 10]. We believe that this MRI evaluation is an important assessment to avoid methodological bias.

We also used a technique of cell labeling based on clinically validated iron oxide particles that allows monitoring the fate of engraftment in vivo. Such a labeling technique has already been used successfully in stem cell therapy to attest the correct delivery of stem cells after intramyocardial or intravenous injection [8–11]. To the best of our knowledge, however, the MRI-based in vivo cell tracking, which enabled us to attest the correct positioning of the patch in front of the infarcted area and the temporal decrease of the patch volume concomitant to the cell infiltration deep into the myocardial wall, has not been reported previously, upon engraftment of ESCs in a 3D fibrin-based cardiopatch.

Of note, the observed larger patch volume on sham animals compared with infarcted animals suggests in those latter an increased degradation, likely related to the inflammatory reaction driven by the infarct. Importantly, the absence of significant alterations in local and global heart function in noninfarcted animals compared with hearts without cardiopatches indicates little to no adverse safety effects of grafting fibrin-based cardiopatches per se. Moreover, no growing tissue or even sign of tumoral growth was observed at the surface of the hearts (data not shown). Although the absence of teratoma should be ascertained at much longer time points, presently we can only speculate that teratoma may not have occurred given the reduced cell number used at start (300,000), the peculiar local microenvironment in which our cells were seeded (homogenously distributed in a 3D fibrin patch grafted on the epicardium), and/or possible paracrine and autocrine factors coming from the ESCs, and/or the cardiac microenvironment.

One of the limitations of using SPIO labeling is the difficulty of differentiating the MR contrast generated by SPIO particles within macrophages from iron remaining inside transplanted cells [54]. Several studies have demonstrated that SPIO-labeled detection is accurate shortly after the engraftment and labeling, but it becomes nonspecific at 1 month with the persistence of iron oxides inside the macrophages at the site of engraftment [54]. In our study, the rationale for using SPIO alone or SPIO-loaded cells was first to image cardiopatches in vivo and then to differentiate ESC-derived cells with a cardiac fate (SPIO and MEF2 positive), still detectable at 1 month, from iron deposition by dead ESC-derived cells or from infiltrating macrophages with

Table 2A. Circumferential strain values assessed for the remote, adjacent (50% infarcted), and infarcted sectors, as well as for the endocardium, midwall, and epicardium, as a function of time in myocardial infarcted hearts treated or not with Cell-patches

	Days		
	2	7	45
Sham group			
Remote ($n = 70$)			
Endo	−0.36 ± 0.08	−0.36 ± 0.05	−0.37 ± 0.06
Mid	−0.25 ± 0.05	−0.25 ± 0.03	−0.26 ± 0.03
Epi	−0.18 ± 0.03	−0.18 ± 0.02	−0.18 ± 0.02
MI group			
Mid	−0.18 ± 0.05	−0.19 ± 0.09	−0.19 ± 0.02
Epi	−0.14 ± 0.04	−0.15 ± 0.05	−0.15 ± 0.02
Adjacent ($n = 46$)			
Endo	−0.16 ± 0.06	−0.18 ± 0.06	−0.18 ± 0.05
Mid	−0.10 ± 0.04	−0.12 ± 0.05	−0.13 ± 0.03
Epi	−0.08 ± 0.03	−0.10 ± 0.05	−0.12 ± 0.03
Infarcted ($n = 36$)			
Endo	−0.13 ± 0.05	−0.16 ± 0.08	−0.13 ± 0.04
Mid	−0.08 ± 0.04	−0.11 ± 0.06	−0.11 ± 0.04
Epi	−0.07 ± 0.04	−0.09 ± 0.05	−0.09 ± 0.04
MI + Cell-patch			
Remote ($n = 30$)			
Endo	−0.29 ± 0.09	−0.30 ± 0.04	−0.31 ± 0.06
Mid	−0.21 ± 0.05	−0.22 ± 0.05	−0.23 ± 0.03
Epi	−0.16 ± 0.03	−0.16 ± 0.03	−0.18 ± 0.02
Adjacent ($n = 16$)			
Endo	−0.18 ± 0.09	−0.18 ± 0.07	−0.23 ± 0.08
Mid	−0.12 ± 0.07	−0.13 ± 0.05	−0.16 ± 0.03
Epi	−0.09 ± 0.06	−0.11 ± 0.04	−0.13 ± 0.04
Infarcted ($n = 19$)			
Endo	−0.15 ± 0.04	−0.16 ± 0.04	−0.14 ± 0.05
Mid	−0.10 ± 0.04	−0.11 ± 0.04	−0.12 ± 0.04
Epi	−0.09 ± 0.05	−0.09 ± 0.03	−0.11 ± 0.04

Table 2B. *p* values of ANOVA with a repeated-measures design estimating the effect of Cell-patches on the myocardial strains in the 3 layers of the wall, adjusted for time, slice level, and type of sectors (remote, adjacent, and infarcted) and their full interactions; no interaction terms were significant

	Effects							
	Treatment[b]			Time Slice		Sector type[c]		
Strain layer[a]	Overall	Sham group	MI group	Overall	Overall	Overall	Adjacent	Infarct
Endo	<0.001[d]	0.029[d]	0.008[d]	0.63	0.699	<0.001[d]	<0.001[d]	<0.001[d]
Mid	<0.001[d]	0.221	0.026[d]	0.246	0.938	<0.001[d]	<0.001[d]	<0.001[d]
Epi	0.002[d]	0.7	0.072	0.058	0.189	0.002[d]	<0.001[d]	<0.001[d]

Sham group = grouping N, N + Iron-patch, and N + Cell-patch values. MI group = grouping MI and MI + Iron-patch values. *n* = number of sectors analyzed.

[a]Circumferential strain measured in the subendocardium (Endo), midwall (Mid), and subepicardium (Epi) layer of the left ventricular wall.

[b]The MI + cell group is used as reference for the pairwise group comparison of the ANOVA with a repeated-measure design.

[c]The remote sectors are used as reference for the pairwise group comparison of the ANOVA with a repeated-measure design.

[d]Significant value.

Abbreviations: Endo, endocardium; Epi, epicardium; MI, myocardial infarction; Mid, midwall; N, normal.

phagocytosed SPIO. The good correlation, in Cell-patch conditions, between iron staining and cardiac-committed cells was encouraging, as, in addition, we did not observe a significant number of infiltrating macrophages at their place (data not shown). Obviously, future experiments should address histology at earlier time points, as well as the use of different cardiogenic cells (from ESC or non-ESC sources), either immunocompatible or in the presence of mild immunosuppressive treatments. Differences in particle detection across time may be explained by the different types of iron oxides (ferumoxides in previous studies versus ferucarbotran in the present study) with respect to coating and size [55]. Such pharmokinetic difference between both types of iron oxides was recently observed in a model of pancreatic islet transplant in rats [56]. Further studies, however, are needed to assess the clearance of Resovist-loaded cells because an improved specificity of labeling with this contrast agent is suggested.

The mode of patch delivery is under test by multiple laboratories. Zimmermann et al. have performed extensive work on collagen ring-shape gels in which cardiomyocyte alignment and force generation can be favored by stretching [24]. Using such a type of approach, however, deep cell infiltration in the infarcted area may not be achievable, and long-term experiments remain to be done to address the functional interaction between the 3D constructs and the infarcted areas. Instead, the use of fibrin hydrogels (with fast degradability already 1 week postgrafting) relies more on cell migration and self-organization propensity of cells delivered at the epicardium side, which may be highly dependent on neoangiogenesis for survival in ischemic tissues. In agreement with our approach, recently fibrin patches have been successfully applied for the engraftment of human ESC-derived vascular cells in large animal hearts [57]. The concomitant delivery of both cell types is thus highly appealing.

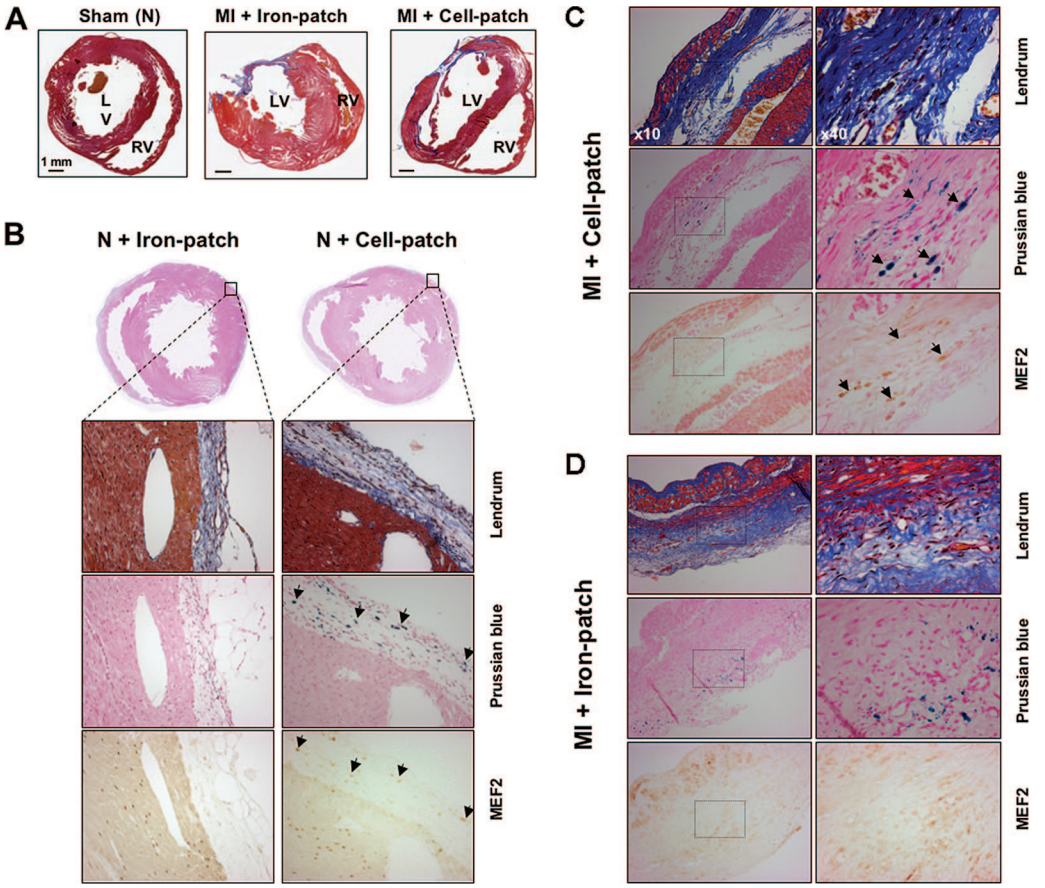

Figure 4. Histological analysis at day 45 of rat hearts transplanted with fibrin patches containing either superparamagnetic iron oxide (SPIO) nanoparticles (Iron-patch) or bone morphogenetic 2-primed, SPIO-loaded mouse embryonic stem cells (mESCs) (Cell-patch). **(A):** Representative Lendrum stains of transverse heart sections showing the remodeling of the myocardium after permanently occluding the left anterior descending coronary artery, displaying muscular fibers in red, collagen in blue, and fibrin in orange. Effects of different treatments are compared: sham-operated heart with a normal morphology (left), typical infarcted hearts with engrafted Iron-patch (center) or Cell-patch (right). A large part of the anterolateral wall is reduced to a paper-thin fibrous layer. The left ventricular wall is hypertrophied in the Iron-patch condition, in contrast to infarcted rats treated with Cell-patch (right). Scale bars = 1 mm. **(B):** Immunohistochemical analysis of normal heart sections at day 45 after the engraftment from the Iron-patch group (left) and the Cell-patch group (right). Landrum staining confirmed the presence of fibrotic tissue for both groups at the periphery of the left ventricle muscle where the patch was positioned. Iron presence is indicated by the Prussian blue coloration. Anti-MEF2 staining revealed the presence of ESC-committed cardiomyocytes in the epicardial area, as well as of rat cardiomyocytes in the left ventricular wall. Arrows indicate examples of cells positive for both MEF2 and Prussian blue staining in consecutive sections. **(C):** Histological analysis of the Cell-patch engraftment in the infarcted rat hearts. Collagen staining of the infarcted left ventricle wall (blue, collagen; red, cardiac muscle). Tissue sections in the lower row (Prussian blue) are consecutive to the sections in the upper row (MEF2). Identification of SPIO-loaded mESCs colonizing the left ventricular wall, as demonstrated by colocalization of Prussian blue (arrows) and MEF2-staining (orange, arrows) in consecutive sections. **(D):** Analysis of Iron-patch engraftment in infarcted rat hearts. Collagen staining of the infarcted left ventricle wall (blue, collagen; red, cardiac muscle). No consistent colocalization could be detected between SPIO nanoparticles, likely incorporated into the tissue via inflammatory cells, and the MEF2-positive staining. Abbreviations: MEF2, myocyte enhancer factor 2; MI, myocardial infarction; N, normal.

Our data suggest that both (a) transplanted cell contribution to neovascularization, possibly through endogenous recruitment of CD31-positive cells, or even via in situ ESC differentiation toward vascular-type cells, and (b) paracrine signaling cues may have contributed to preserving the viability of host cardiomyocytes and thereby the heart function. Indeed, the Cell-patch effect is seen already at day 2 (the first assessed time point in our study). The fact that CD31-positive vessels into the engrafted area did not show nanoparticle-enriched cells indicates either that the endothelial cells did not originate from ESCs or that the nanoparticles were diluted below detection level by extensive cell division. Regardless of this, the observed extensive capillary network, absent in sham-operated hearts, suggests that ESC engraftment per se is capable of inducing the formation of new capillaries. Clearly, these hypotheses remain to be investigated in future studies using genetically tagged cells, as well as techniques to assess the possible enhanced preservation of host tissue viability.

The importance of paracrine-signaling effects has been also suggested by recent key studies transplanting hESC-derived cardiomyocytes into infarcted hearts [18, 58]. Cardiac function was improved despite the fact that many of the donor cardiomyocytes in those studies were not in direct contact with the host cardiomyocytes, complicating electrophysiological coupling or even making it impossible. Furthermore, paracrine factors may not only enhance angiogenesis but also modulate inflammatory responses, which are both relevant processes in infarcted hearts. In future studies based on robust and standardized MRI tools, we

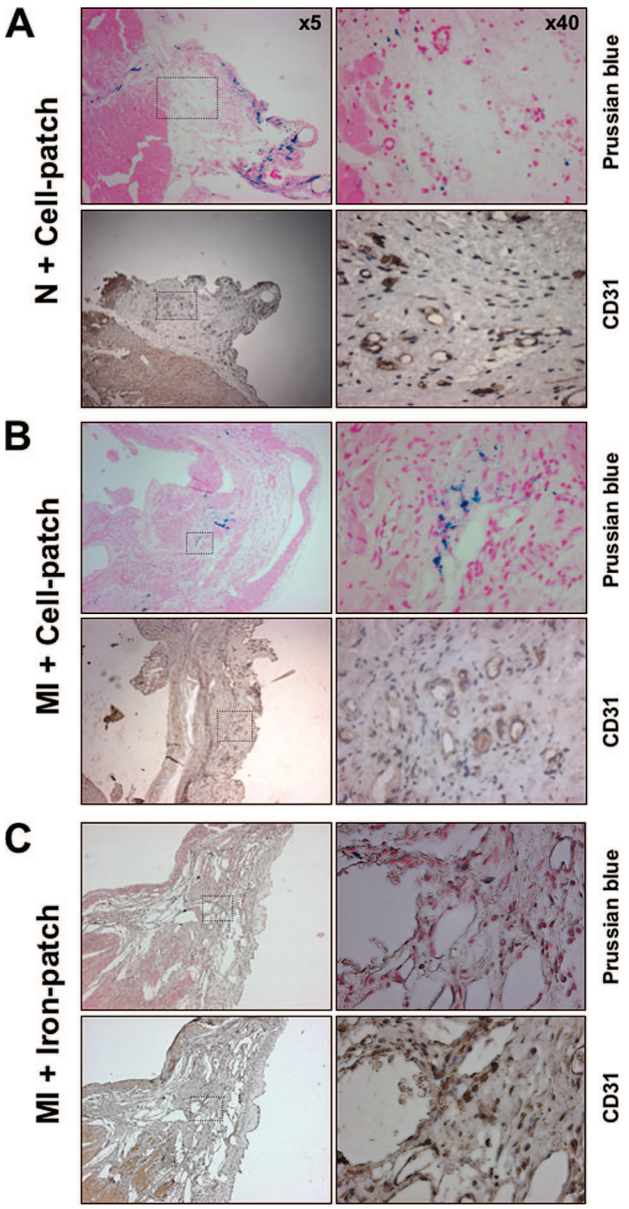

Figure 5. Histological analysis of vascular-like structures (CD31-positive) in the scar area of infarcted rat hearts, 45 days after surgically inducing myocardial infarction. Infarcted hearts treated with superparamagnetic iron oxide (SPIO)-loaded mouse embryonic stem cells (**[B]**, MI + Cell-patch) or patch seeded with SPIO-loaded patch (**[C]**, MI + Iron-patch) were compared with noninfarcted rats (**[A]**, N + Cell-patch). CD31-positive cells were observed only in the Cell-patch condition, in the vicinity of grafted cells, but were not positive for Prussian blue staining. Abbreviations: MI, myocardial infarction; N, normal.

thus foresee the importance of comparing the impact of different cells sources on the heart function including mesenchymal stem cells, known to mainly exert paracrine effects on the infarcted heart.

Our immunohistochemical data further indicate that the mESC-derived BMP2-primed cells survived over 6 weeks after transplantation, even in the absence of immune suppression, as previously reported by others [59–61]. Although preclinical studies using hESC-derived cardiomyocytes demonstrated that noncardiomyocyte donor cells did not survive when implanted into the center of the infarct [52], we may not spare the use of secure selection methods to discard residual pluripotent cells in clinical settings [40, 62, 63]. Clearly, the issues of using mild immunosuppressive treatments or, optimally, immunocompatible cells (heart-derived progenitors [64], patient-derived induced pluripotent stem cells), together with an optimal cell delivery format, remain to be correctly addressed for a successful clinical translation into humans. Ultimately, the coinjection of other cell types relevant to tissue repair (that is, cardiac fibroblasts and endothelial progenitors), or even passive or elective recruitment of endogenous cells participating to tissue remodeling, will have to be investigated in future studies.

Conclusion

In summary, our study demonstrates that cell engraftment via fibrin-based patches represents a promising therapeutic approach to achieve efficient cell implantation and improved global and regional cardiac function. Therefore, native or functionalized hydrogels, whether prepared from natural (such as fibrin [38]) or synthetic hydrophilic biocompatible polymers (such as PEG [9, 28]) may thus be a suitable choice to bring securely selected cardio-regenerating cells, as well as vascular progenitors and/or neoangiogenic factors, first into large animal testing and ultimately into clinical trials.

Acknowledgments

We are grateful to Qing He and M. Manu Costa for their help and expertise with animal model and surgical techniques. This work was supported in part by the Leenaards Foundation and the Swiss National Science Foundation FNS (grant numbers 4046-058712 and PP00B-68778/1). P.M. is supported by grants from the Swiss National Science Foundation (310030_141162, CR32I3_129987) and the European Union (BETAIMAGE 222980; IMIDIA, C2008-T7). W.B. is currently affiliated with Beijing Hospital of the Ministry of Healthy, Emergency Department, Beijing, People's Republic of China; P.Z. is currently affiliated with Roche Diagnostics Ltd., Rotkreuz, Switzerland; T.P.K. is currently affiliated with Hoffman-La Roche, Translational Research Sciences, Nutley, New Jersey.

Author Contributions

J.-P.V.: conception and design, financial support, data analysis and interpretation, manuscript writing, final approval of manuscript; M.H., M.L.-C.: collection and assembly of data, data analysis and interpretation, help in manuscript writing; W.B., K.M.-A.: collection of data; P.M.: assembly of data, data analysis and interpretation; S.G.: data analysis; P.Z.: conception and design, methodological help; T.P.K.: help in manuscript writing and revision; F.H.: data analysis and interpretation; J.A.H.: provision of study material, biomaterial expertise support; M.E.J.: conception and design, administrative and financial support, data collection and assembly, data analysis and interpretation, manuscript writing, final approval of manuscript.

Disclosure of Potential Conflicts of Interest

The authors indicate no potential conflicts of interest.

References

1 Thom T, Haase N, Rosamond W et al. Heart disease and stroke statistics–2006 update: A report from the American Heart Association Statistics Committee and Stroke Statistics Subcommittee. Circulation 2006;113:e85–e151.

2 Anversa P, Leri A, Kajstura J. Cardiac regeneration. J Am Coll Cardiol 2006;47:1769–1776.

3 Parmacek MS, Epstein JA. Cardiomyocyte renewal. N Engl J Med 2009;361:86–88.

4 Schuleri KH, Amado LC, Boyle AJ et al. Early improvement in cardiac tissue perfusion due to mesenchymal stem cells. Am J Physiol Heart Circ Physiol 2008;294:H2002–H2011.

5 Terrovitis J, Bulte J, Sarvananthan S et al. Magnetic resonance imaging of ferumoxide-labeled mesenchymal stem cells seeded on collagen scaffolds-relevance to tissue engineering. Tissue Eng 2006;12:2765–2775.

6 Ye Y, Bogaert J. Cell therapy in myocardial infarction: Emphasis on the role of MRI. Eur Radiol 2008;18:548–569.

7 Flynn A, O'Brien T. Stem cell therapy for cardiac disease. Expert Opin Biol Ther 2011;11:177–187.

8 Qiao H, Zhang H, Yamanaka S et al. Long-term improvement in postinfarct left ventricular global and regional contractile function is mediated by embryonic stem cell-derived cardiomyocytes. Circ Cardiovasc Imaging 2011;4:33–41.

9 Kraehenbuehl TP, Ferreira LS, Hayward AM et al. Human embryonic stem cell-derived microvascular grafts for cardiac tissue preservation after myocardial infarction. Biomaterials 2011;32:1102–1109.

10 Carr CA, Stuckey DJ, Tan JJ et al. Cardiosphere-derived cells improve function in the infarcted rat heart for at least 16 weeks—an MRI study. PLoS One 2011;6:e25669.

11 Au KW, Liao SY, Lee YK et al. Effects of iron oxide nanoparticles on cardiac differentiation of embryonic stem cells. Biochem Biophys Res Commun 2009;379:898–903.

12 Orlic D, Hill JM, Arai AE. Stem cells for myocardial regeneration. Circ Res 2002;91:1092–1102.

13 Passier R, van Laake LW, Mummery CL. Stem-cell-based therapy and lessons from the heart. Nature 2008;453:322–329.

14 Joggerst SJ, Hatzopoulos AK. Stem cell therapy for cardiac repair: Benefits and barriers. Expert Rev Mol Med 2009;11:e20.

15 Rangappa S, Makkar R, Forrester J. Review article: Current status of myocardial regeneration: New cell sources and new strategies. J Cardiovasc Pharmacol Ther 2010;15:338–343.

16 Segers VF, Lee RT. Stem-cell therapy for cardiac disease. Nature 2008;451:937–942.

17 Laflamme MA, Murry CE. Heart regeneration. Nature 2011;473:326–335.

18 Laflamme MA, Chen KY, Naumova AV et al. Cardiomyocytes derived from human embryonic stem cells in pro-survival factors enhance function of infarcted rat hearts. Nat Biotechnol 2007;25:1015–1024.

19 Suter DM, Cartier L, Bettiol E et al. Rapid generation of stable transgenic embryonic stem cell lines using modular lentivectors. Stem Cells 2006;24:615–623.

20 Freund C, Mummery CL. Prospects for pluripotent stem cell-derived cardiomyocytes in cardiac cell therapy and as disease models. J Cell Biochem 2009;107:592–599.

21 Mooney DJ, Vandenburgh H. Cell delivery mechanisms for tissue repair. Cell Stem Cell 2008;2:205–213.

22 Gaballa M, Sunkomat J, Thai H et al. Grafting an acellular 3-dimensional collagen scaffold onto a non-transmural infarcted myocardium induces neo-angiogenesis and reduces cardiac remodeling. J Heart Lung Transplant 2006;25:946–954.

23 Leor J, Gerecht-Nir S, Cohen S et al. Human embryonic stem cell transplantation to repair the infarcted myocardium. Heart 2007;93:1278-1284.

24 Zimmermann WH, Melnychenko I, Wasmeier G et al. Engineered heart tissue grafts improve systolic and diastolic function in infarcted rat hearts. Nat Med 2006;12:452–458.

25 Christman KL, Lee RJ. Biomaterials for the treatment of myocardial infarction. J Am Coll Cardiol 2006;48:907–913.

26 Caspi O, Lesman A, Basevitch Y et al. Tissue engineering of vascularized cardiac muscle from human embryonic stem cells. Circ Res 2007;100:263–272.

27 Lesman A, Habib M, Caspi O et al. Transplantation of a tissue-engineered human vascularized cardiac muscle. Tissue Eng Part A 2010;16:115–125.

28 Kraehenbuehl TP, Langer R, Ferreira LS. Three-dimensional biomaterials for the study of human pluripotent stem cells. Nat Methods 2011;8:731–736.

29 Shimizu T, Yamato M, Isoi Y et al. Fabrication of pulsatile cardiac tissue grafts using a novel 3-dimensional cell sheet manipulation technique and temperature-responsive cell culture surfaces. Circ Res 2002;90:e40.

30 Miyahara Y, Nagaya N, Kataoka M et al. Monolayered mesenchymal stem cells repair scarred myocardium after myocardial infarction. Nat Med 2006;12:459–465.

31 Vacanti JP, Langer R, Upton J et al. Transplantation of cells in matrices for tissue regeneration. Adv Drug Deliv Rev 1998;33:165–182.

32 Zammaretti P, Jaconi M. Cardiac tissue engineering: Regeneration of the wounded heart. Curr Opin Biotechnol 2004;15:430–434.

33 Dai W, Wold LE, Dow JS et al. Thickening of the infarcted wall by collagen injection improves left ventricular function in rats: A novel approach to preserve cardiac function after myocardial infarction. J Am Coll Cardiol 2005;46:714–719.

34 Christman KL, Vardanian AJ, Fang Q et al. Injectable fibrin scaffold improves cell transplant survival, reduces infarct expansion, and induces neovasculature formation in ischemic myocardium. J Am Coll Cardiol 2004;44:654–660.

35 Zimmermann WH. Tissue engineering: Polymers flex their muscles. Nat Mater 2008;7:932–933.

36 Engelmayr GC, Jr., Cheng M, Bettinger CJ et al. Accordion-like honeycombs for tissue engineering of cardiac anisotropy. Nat Mater 2008;7:1003–1010.

37 Davis ME, Hsieh PC, Grodzinsky AJ et al. Custom design of the cardiac microenvironment with biomaterials. Circ Res 2005;97:8–15.

38 Ehrbar M, Djonov VG, Schnell C et al. Cell-demanded liberation of VEGF121 from fibrin implants induces local and controlled blood vessel growth. Circ Res 2004;94:1124–1132.

39 Urech L, Bittermann AG, Hubbell JA et al. Mechanical properties, proteolytic degradability and biological modifications affect angiogenic process extension into native and modified fibrin matrices in vitro. Biomaterials 2005;26:1369–1379.

40 He Q, Trindade PT, Stumm M et al. Fate of undifferentiated mouse embryonic stem cells within the rat heart: Role of myocardial infarction and immune suppression. J Cell Mol Med 2009;13:188–201.

41 Li J, Stouffs M, Serrander L et al. The NADPH oxidase NOX4 drives cardiac differentiation: Role in regulating cardiac transcription factors and MAP kinase activation. Mol Biol Cell 2006;17:3978–3988.

42 Ménard C, Hagege AA, Agbulut O et al. Transplantation of cardiac-committed mouse embryonic stem cells to infarcted sheep myocardium: A preclinical study. Lancet 2005;366:1005–1012.

43 Meyer N, Jaconi M, Landopoulou A et al. A fluorescent reporter gene as a marker for ventricular specification in ES-derived cardiac cells. FEBS Lett 2000;478:151–158.

44 Kraehenbuehl TP, Zammaretti P, Van der Vlies AJ et al. Three-dimensional extracellular matrix-directed cardioprogenitor differentiation: Systematic modulation of a synthetic cell-responsive PEG-hydrogel. Biomaterials 2008;29:2757–2766.

45 Reynolds ES. The use of lead citrate at high pH as an electron-opaque stain in electron microscopy. J Cell Biol 1963;17:208–212.

46 Ivancevic M, Daire J, Hyacinthe J et al. High-resolution complementary spatial modulation of magnetization (CSPAMM) rat heart tagging on a 1.5 Tesla Clinical Magnetic Resonance System: A preliminary feasibility atudy. Invest Radiol 2007;42:204–210.

47 Daire J, Hyacinthe J, Tatar I et al. In vivo myocardial infarct area at risk assessment in the rat using manganese enhanced magnetic resonance imaging (MEMRI) at 1.5T. Magn Reson Med 2008;59:1422–1430.

48 Daire J, Jacob J, Hyacinthe J et al. Cine and tagged MRI in normal rat at 1.5T: A rest and stress study. J Cardiovasc Magn Reson 2008;10:48.

49 Jacob J, Vachier C, Morel J et al. Extrema temporal chaining: A new method for computing the 2D-displacement field of the heart from tagged MRI. Lect Notes Comput Sci 2006;4179:897–908.

50 Lendrum AC, Fraser DS, Slidders W et al. Studies on the character and staining of fibrin. J Clin Pathol 1962;15:401–413.

51 Chaudeurge A, Wilhelm C, Chen-Tournoux A et al. Can magnetic targeting of magnetically labeled circulating cells optimize intramyocardial cell retention? Cell Transplantation 2011 [Epub ahead of print].

52 van Laake LW, Passier R, den Ouden K et al. Improvement of mouse cardiac function by hESC-derived cardiomyocytes correlates with vascularity but not graft size. Stem Cell Res 2009;3:106–112.

53 Stuckey DJ, Ishii H, Chen QZ et al. Magnetic resonance imaging evaluation of remodeling by cardiac elastomeric tissue scaffold biomaterials in a rat model of myocardial infarction. Tissue Eng Part A 2010;16:3395–3402.

54 Terrovitis J, Stuber M, Youssef A et al. Magnetic resonance imaging overestimates ferumoxide-labeled stem cell survival after transplantation in the heart. Circulation 2008; 117:1555–1562.

55 Corot C, Robert P, Idee JM et al. Recent advances in iron oxide nanocrystal technology for medical imaging. Adv Drug Deliv Rev 2006; 58:1471–1504.

56 Ris F, Lepetit-Coiffe M, Meda P et al. Assessment of human islet labeling with clinical grade iron nanoparticles prior to transplantation for graft monitoring by MRI. Cell Transplant 2010;19:1573–1585.

57 Ye Z, Zhou Y, Cai H et al. Myocardial regeneration: Roles of stem cells and hydrogels. Adv Drug Deliv Rev 2011;63:688–697.

58 van Laake LW, Passier R, Doevendans PA et al. Human embryonic stem cell-derived cardiomyocytes and cardiac repair in rodents. Circ Res 2008;102:1008–1010.

59 Behfar A, Zingman LV, Hodgson DM et al. Stem cell differentiation requires a paracrine pathway in the heart. FASEB J 2002;16:1558–1566.

60 Hodgson DM, Behfar A, Zingman LV et al. Stable benefit of embryonic stem cell therapy in myocardial infarction. Am J Physiol Heart Circ Physiol 2004;287:H471–H479.

61 Raida M, Clement JH, Leek RD et al. Bone morphogenetic protein 2 (BMP-2) and induction of tumor angiogenesis. J Cancer Res Clin Oncol 2005;131:741–750.

62 Cao F, van der Bogt KE, Sadrzadeh A et al. Spatial and temporal kinetics of teratoma formation from murine embryonic stem cell transplantation. Stem Cells Dev 2007;16:883–891.

63 Nussbaum J, Minami E, Laflamme MA et al. Transplantation of undifferentiated murine embryonic stem cells in the heart: Teratoma formation and immune response. FASEB J 2007;21:1345–1357.

64 Bolli R, Chugh AR, D'Amario D et al. Cardiac stem cells in patients with ischaemic cardiomyopathy (SCIPIO): Initial results of a randomised phase 1 trial. Lancet 2011;378: 1847-1857.